WILEY

A variational rigid-block modeling approach to nonlinear elastic and kinematic analysis of failure mechanisms in historic masonry structures subjected to lateral loads

Francesco P. A. Portioli[1] | **Michele Godio**[2] | **Chiara Calderini**[3] | **Paulo B. Lourenço**[4]

[1] Department of Structures for Engineering and Architecture, University of Naples Federico II, Naples, Italy

[2] RISE Research Institutes of Sweden, Borås, Sweden

[3] Department of Civil, Chemical and Environmental Engineering, University of Genoa, Genoa, Italy

[4] Department of Civil Engineering, ISISE, University of Minho, Guimarães, Portugal

Correspondence
Francesco P. A. Portioli, Department of Structures for Engineering and Architecture, University of Naples Federico II, via Forno Vecchio 36, Naples 80134, Italy.
Email: fportiol@unina.it

Abstract

Displacement-based methods contained in recent standards for seismic safety assessment require the determination of the full nonlinear pushover curve for local failure mechanisms in historic masonry structures. This curve should reflect both the initial elastic behavior and the rigid body behavior after the activation of rocking. In this work, a rigid block model is proposed for the displacement-based seismic assessment of local collapse mechanisms of these structures. Masonry is modeled as an assemblage of two-dimensional rigid blocks in contact through frictional interfaces. Two types of contact models are formulated to capture, respectively, the pre and postpeak branches of the pushover curve: a unilateral elastic contact model, capturing the initial nonlinear behavior up to the force capacity of the structure, corresponding to the activation of the collapse mechanism, and a rigid contact model with finite friction and compressive strength, which describes the rigid-body rocking behavior up to the attainment of the displacement capacity of the structure. Tension-only elements are also implemented to model strengthening interventions with tie-rods. The contact problems associated with the elastic and rigid contact models are formulated using mathematical programming. For both models, a sequential solution procedure is implemented to capture the variation of the load multiplier with the increasing deformation of the structure (P–Δ effect). The accuracy of the modeling approach in reproducing the pushover curve of masonry panels subjected to horizontal seismic loads is evaluated on selected case studies. The solution is first tested against hand calculations, existing analytical models, and distinct element simulations. Then, comparisons against experimental tests follow. As a final application, the failure mechanism and pushover curve of a triumphal masonry arch are predicted by the model and its seismic assessment is performed according to codified force- and displacement-based methods, demonstrating the adequacy of the proposed tool for practice.

1 | INTRODUCTION

Historic masonry structures develop local failure mechanisms when subjected to earthquakes. Such mechanisms may involve single structural elements, up to entire portions of building. No matter the "size" of the failure mechanism, the evaluation of its impact on the damage, life safety and, more generally, the seismic performance is a key issue in the structural assessment of historic constructions, as, in most cases, can affect the overall stability.

The seismic assessment of the local failure mechanisms in masonry structures is challenging in many ways: first, in the prediction of the mechanism itself, which, in practice, is left to the analyst's choice; second, in the evaluation of the mass participating in the mechanism; third, in the implementation of correct boundary conditions, which are not necessarily the same from the initiation to the full development of the mechanism, and, in some circumstances, may evolve with it.[1] In current codes, the seismic assessment of the local collapse mechanisms in masonry structures is addressed by force- and displacement-based methods. These methods make use of, respectively, the force and the displacement capacity of the structure to perform the "final check" and determine its seismic performance.[2] The Italian technical standard[3,4] comprises both methods for the life-safety limit-state verification of masonry structures. Important differences may be found between the methods,[5] being the displacement-based method scale dependent, while the force-based method not.[6] Studies performed using the previous version of the standard[7] show that the displacement-based method appears to be more robust, accurate, and safer than the force-based method in predicting the acceleration capacity leading the structure to failure.[8]

The displacement-based method recommended in the Italian technical standard is based on the derivation of the pushover curve.[4] According to this standard, this curve is bilinear and can be generally obtained by assuming a linear elastic branch for the prepeak behavior, followed by a descending postpeak branch describing the rigid-body behavior corresponding to the failure mechanism. The pushover curve is then used to evaluate the capacity curve corresponding to an equivalent, single-degree-of-freedom (SDOF) system to predict the acceleration that leads the structure to failure by comparison of its displacement capacity with the displacement demand, in analogy to the capacity spectrum method.[1,9,10] The use of pushover curves and capacity spectrum methods for the seismic assessment of local failure mechanism was validated against static and dynamic tests in the case of vertically spanning walls, arch piers systems, and U-shaped assemblages consisting of a façade and two transverse walls.[11–13] Parametric studies and comparisons with time history analyses showed that the accuracy of these methods is sensitive to the period of the equivalent SDOF system, corresponding to a given displacement capacity, and can be excessively conservative unless small periods are considered.[10] Moreover, the dispersion of the results is also affected by the choice of the intensity measure, such as peak ground velocity or peak ground acceleration, the last one being commonly adopted in the standards.[2] In this study, the methods contained in the new version of the Italian technical standard are implemented.[3,4]

The portion of the structure involved in the collapse mechanism undergoes moderate deflections, that is, out-of-plane displacements whose magnitude is of the order of the element thickness. Modeling approaches incorporating geometric nonlinearity, that is, P−Δ effects, are thus needed. In this context, various modeling approaches have been proposed in the literature, which can be conveniently used for the analysis of local failure mechanisms. Those generally comprise analytical models,[14–17] homogeneous and discontinuous finite element models,[18–21] macroelement models,[22–24] as well as applied, distinct element and nonsmooth contact dynamics models.[25–33] Multistep models and CAD tools based on macro-modeling approaches have been also proposed.[5,34] Among these methods, discontinuous modeling approaches appear to be particularly suitable for the analysis of the local collapse mechanisms, mainly thanks to the discretization and formulations adopted, which allow the activation and evolution of the mechanisms to be followed closely and without a-priori assumptions, making them adapted to the assessment methods included in the standards.[4]

Rigid block models present attractive aspects from the computational point of view when compared to other discontinuous modeling approaches, such as the distinct element method.[35] These features can be mainly ascribed to the form and the solution of the variational formulation, which is used for the problems governing the response at the contact interfaces between the blocks. In particular, when no-tension frictional interfaces are considered, as it is the case of historic masonry structures where the contribution of tensile and cohesive strength is often uncertain and negligible, inequalities

and complementarity conditions can be used to express in a direct and compact form the unilateral behavior associated with contact joints. Importantly, when an associative behavior is assumed for displacement rates at contact interfaces, it can be shown that the systems of governing equations can be uncoupled into dual optimization problems, following the classic approaches of limit analysis, generally corresponding to a force-based and to a displacement-based optimization problem. The possibility to solve only one of the corresponding optimization problems (e.g., the force-based problem) and to obtain the solution of the dual problem from Lagrange multipliers associated with the solution of the same optimization problem––thus obtaining in a single run both the static and kinematic variables––and the availability of efficient solution procedures for mathematical programming makes this approach particularly convenient in terms of CPU time and simplicity of implementation in a structural analysis code.

At present, most of the rigid block models proposed in the literature are based on classical limit analysis formulations, which allow only the force capacity of the structure to be estimated.[18,36–43] This shortcoming, which is related to the fact that the load multiplier is computed on the initial structural configuration and therefore related to the activation of the failure mechanism but not on its evolution, prevents their use in displacement-based methods currently contained in the standards.[4] Recently, rigid block models based on sequential limit analysis and incremental solution procedures have been proposed to consider the effects of large displacements. However, these rigid block models have been mainly used for the analysis of settlement induced-failure mechanisms.[44–46] Moreover, those models generally do not comprise the elastic response and, as such, can only be used for the nonlinear kinematic analysis of the mechanisms, that is, for the evaluation of the postpeak rocking behavior.

To overcome these limitations, a 2D rigid block model is proposed in this paper for the pushover analysis of local failure mechanisms in historic masonry structures. The model comprises both the elastic and the rigid-body behaviors required by the standard.[4] The masonry pattern is discretized into an assemblage of rigid blocks interacting at no-tension elastic contact interfaces with finite friction and compression strength. As such, the proposed approach relies on few model parameters, that are the stiffness, the coefficient of friction at contact interfaces, and the compressive strength, together with the rigid block and load configuration. Two contact models are implemented: a unilateral elastic no-tension model, which allows the initial nonlinear behavior up to the activation of the collapse mechanism to be captured, and a rigid no-tension frictional model with finite compressive strength, which describes the rigid-body rocking behavior corresponding to the evolution of the collapse mechanism up to the attainment of the displacement capacity of the structure. The contact models are formulated through mathematical programming. The resulting formulation makes use of duality between statics and kinematics to uncouple the solution into two distinct force- and displacement-controlled optimization schemes, thus reducing the computational cost. A sequential solution procedure is implemented to solve the optimization problems on the deformed structural configuration, thus considering the P−Δ effects in the construction of the pushover curve.

The approach proposed is primarily suitable for ancient, monumental buildings comprising slender masonry elements, like columns, arches, arch-piers systems and, more generally, out-of-plane loaded walls made of natural stone blocks, with dry or low bond strength mortar joints, which involve collapse modes that are mainly governed by bending and overturning failures.[1] For these cases, in the proposed approach, failures are assumed to occur at the dry joints or at the brick to mortar interface or mortar itself. The failure of masonry units and related failure mechanisms are not comprised in the present formulation. The assumption of no-tension material is accurate only in the case of dry joint masonry. Applications of the proposed approach to masonry with low bond strength mortar joints are conservative and involve a lower level of accuracy, which in general depends on the value of tensile strength and cohesion, on the geometry of the structural element, and on the failure mode considered. For example, in the case of brickwork wall panels with openings[47] and in the case of slender unreinforced masonry walls under lateral loads,[48] it was noted that the tensile strength mainly affects early cracking and the force capacity in the prepeak response. In the case of Ref. 48, a slight influence was observed on the ultimate displacements.

The study is framed with the aim of developing efficient tools based on mathematical programming for the limit equilibrium, large displacement, and time-history analysis of historic masonry structures subjected to seismic actions and settlements.[35,45,49] The key features of the model presented in this study with respect to those contained in the authors' previous works are the ability to consider, within a unified modeling approach: the elastic prepeak behavior of the interfaces, including not only the normal behavior, as done in Ref. 50 for the study of the effects induced by settlements, but also the tangential behavior; a finite compression strength for the nonlinear kinematic analysis of the postpeak behavior, formulated, as for the prepeak behavior, in the large displacement regime; the addition of tie elements, to model seismic strengthening interventions.

The formulation is implemented in the software package MATLAB®. As detailed in the following sections, this allows the rigid block model to be imported from CAD models, while input parameters are assigned by separate functions. The
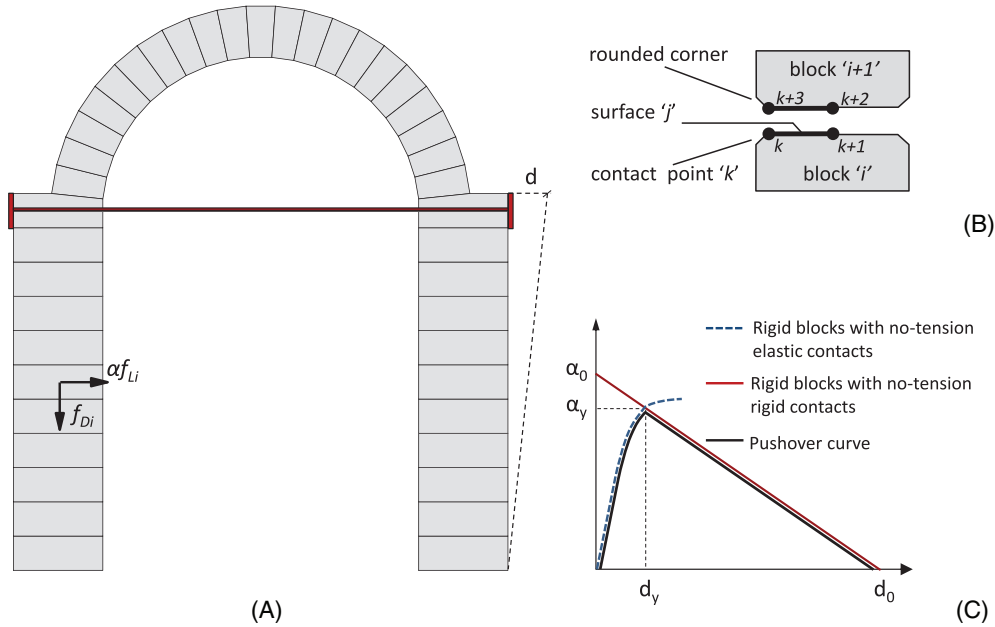
FIGURE 1 (A) Illustration of the rigid block model for a masonry arch strengthened by a tie element, with dead and live loads, considering a factor α as live load multiplier and the displacement d at a control point; (B) rigid block i, surface j, and contact point k; (C) parameters of the pushover curve obtained from the rigid block models with no-tension elastic contacts and no-tension rigid contacts

model is validated extensively against hand calculations, existing analytical solutions, ad-hoc distinct element simulations obtained through the use of a commercial software,[51] and experimental tests from the literature[52,53] and also specifically developed for the present study, which all illustrate the accuracy of the implemented procedure. An application demonstrates its use for the seismic assessment of a masonry structure with curved geometry. It is also worth noticing that, in the proposed approach, multiple contact points can be used to discretize the block edges, while blocks can be appropriately shaped to consider the effect of geometric imperfections. These are two notable features of discontinuous modeling that were show to have an impact on the pushover curves of collapse mechanisms.[54]

Different sections delineate the paper content. Section 2 presents the system of equations governing the rigid block model. In Section 3, the equations are reformulated as mathematical programming problems. The incremental solution procedure used to solve the nonlinear limit analysis problem is presented in Section 4. The validation of the model through numerical benchmarks and experimental tests is illustrated in Sections 5 and 6. In Section 7, the model is used to assess the seismic capacity of a triumphal arch according to codified force- and displacement-based methods.

2 | THE RIGID BLOCK MODELING APPROACH FOR STATIC PUSHOVER ANALYSIS

The proposed model is composed of polygonal rigid blocks which interact at no tension frictional contact interfaces. The model relies on the so-called point contact formulation (also referred to as concave contact formulation in Ref. 55), according to which contact forces are located at the vertices k of the contact surfaces j between the blocks (Figure 1A, B). Notice that, according to the configuration depicted in Figure 1B, four contact points and two contact surfaces are defined for each interface. It is also worth noting that, in the proposed approach, multiple surfaces can be used to discretize block edges and that block corners can be appropriately shaped to consider the effect of geometric imperfections (i.e., rounded corners, see Figure 1B).

In recent studies, bilinear or multilinear models are used in pushover curves to take into account an initial pseudo elastic behavior and a rigid behavior after the activation of the rocking mechanism.[1,9,56,57] In the present study, two kinds of behavior are considered at contact points to evaluate the pre and post peak regimes. These comprise an elastic no-tension behavior and a rigid no-tension behavior with finite friction and compressive strength. The pushover curve is obtained by combining the rising branch corresponding to the former behavior and the descending branch corresponding to the latter behavior (Figure 1C). As such, not only α_0, the live load multiplier at the onset of the mechanism calculated by assuming no-tension rigid contacts, is obtained, but also α_y, the load multiplier corresponding to the force capacity
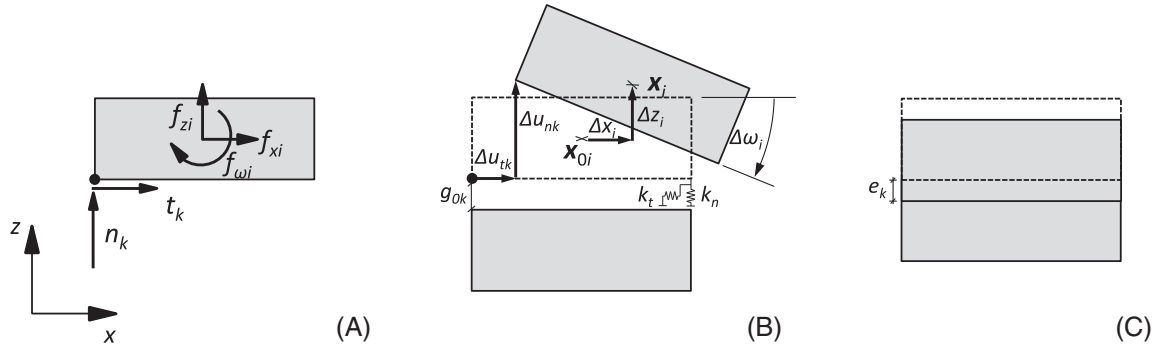
FIGURE 2 (A) External and contact forces; (B) kinematic variables at block centroid i and at contact point k, contact gaps g_{0k}, and contact stiffnesses k_n, k_t; (C) elastic interpenetrations at contact points

of the structure, d_y, the displacement of the control point at the elastic limit, that is, prior to the activation of rocking, and d_0, the displacement capacity of the structure. In both cases, the proposed model considers the effects of geometric nonlinearities by use of an incremental solution procedure, as described in the following sections.

Following the approaches presented in Refs. 35, 38, 58–62, the contact problems corresponding to the two considered behaviors are posed in terms of linear complementarity problems (LCPs).[63] The solution of the contact problems relies, therefore, on the solution of the optimization problems, which are equivalent to these complementarity problems. The optimization problems are solved sequentially in order to compute the variation of the collapse load multiplier with the increasing deformation of the structure. The LCPs stem directly from the system of equilibrium, compatibility, and failure conditions, which govern the behavior of the rigid block assemblage, as briefly illustrated in the following.

The rigid blocks are subjected to external loads with components f_{xi}, f_{zi}, $f_{\omega i}$ (Figure 2). Those are applied to the centroid of rigid block i and are collected, for the whole assemblage, in a $(3b \times 1)$ vector $\boldsymbol{f}$, being b the number of blocks. The other static variables are the tangential and normal forces t_k and n_k acting at the contact points k, which are collected in the $(2c \times 1)$ vector $\boldsymbol{c}$, being c the number of contact points.

The equilibrium equations of the rigid block assemblage at a given configuration $\boldsymbol{x_0}$ can be posed in matrix form as follows, being $\boldsymbol{x_0}$ the $(3b \times 1)$ vector of block centroid coordinates associated with the known initial configuration:

$$\boldsymbol{A_0 c = f},\tag{1}$$

where $\boldsymbol{A_0}$ is the $(3b \times 2c)$ equilibrium matrix, with entries determined on the basis of components of tangential and normal vectors to contact surfaces and on the basis of related moments against blocks centroid for translational and rotational equilibrium conditions, respectively.[35]

The kinematic variables are the unknown relative displacements of the block centroid. They are collected in the vector $\boldsymbol{\Delta x = x - x_0}$. Geometric compatibility between the relative displacements at the block centroids and the displacement rates at contact points can be expressed using the transpose of the equilibrium matrix under the assumption of small displacements, according to the so-called contragradience principle[38]:

$$\boldsymbol{\Delta u = A_0^T \Delta x},\tag{2}$$

where $\boldsymbol{\Delta u}$ is the vector of relative contact displacements collecting components Δu_{tk} and Δu_{nk} for each contact point (Figure 2B).

Failure conditions y_k at the contact point k comprise sliding failure (no-tension) and, in the case of rigid contacts, crushing as well (Figure 3). For the sliding failure, a Coulomb slip criterion is considered:

$$\pm t_k - \mu n_k \leq 0,\tag{3}$$

where μ is the friction coefficient and normal forces are assumed to be positive in compression. In matrix form, sliding and opening failure conditions can be posed as follows:

$$\begin{bmatrix} y_{sk+} \\ y_{sk-} \\ y_{0k} \end{bmatrix} = \begin{bmatrix} 1 & -\mu \\ -1 & -\mu \\ 0 & -1 \end{bmatrix} \begin{bmatrix} t_k \\ n_k \end{bmatrix} \leq \begin{bmatrix} 0 \\ 0 \\ 0 \end{bmatrix},$$
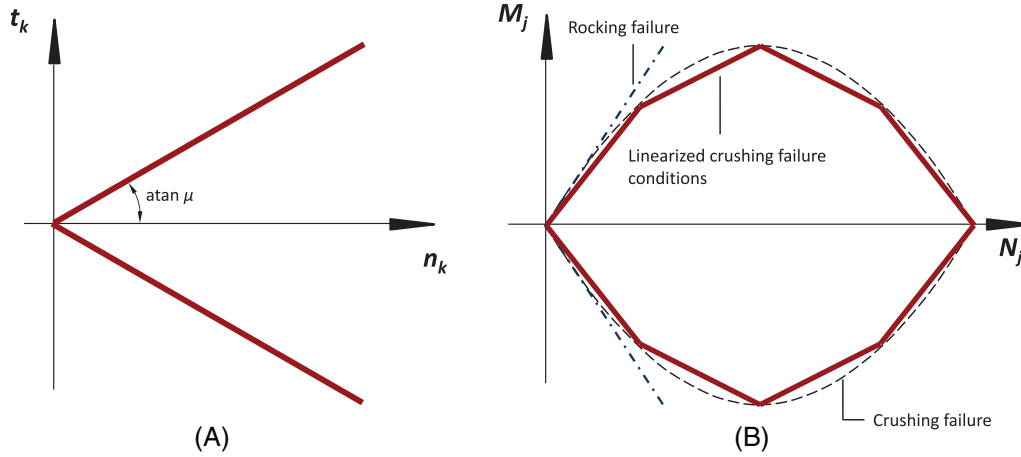
FIGURE 3 (A) Failure surface for pure shear and (B) crushing

or:

$$y_k = Y_k^{\mathrm{T}} \, c_k \leq \mathbf{0}_k. \tag{4}$$

In the case of the rigid contact formulation, in addition to the simple opening failure conditions associated with no tension and infinite compressive strength ($n_k \geq 0$, i.e., rocking failure), crushing failure conditions are included. In this case, a piecewise linearization of the quadratic domain corresponding to the classic stress block assumption is considered in the space of the contact force resultants M_j, N_j (Figure 3B), following the approaches presented in Refs. 64 and 65. For the whole structure, the failure conditions can be written in matrix form as:

$$y = Y^{\mathrm{T}} c - r \leq 0, \tag{5}$$

where Y^{T} is the matrix of failure conditions and r is the vector of constant terms associated with crushing failure conditions which correspond, in the M_j, N_j space, to the distance of the limit planes from the origin. The validity of this approach is investigated in the next sections against analytical solutions.

Similar conditions are formulated for the end nodes of the tie element. In this case, a tension-only behavior is considered for the element, imposing finite values of plastic strength to the normal force component at nodes. Although the element resists to axial force only, finite values are also considered for tangential force components. This is because, in the assembling procedure that was implemented for matrices, two force components are considered by default at each contact node, that is, the normal and the tangential force. As such, the matrix of failure conditions at an end point k of the tie element is formulated as follows:

$$\begin{bmatrix} y_{sk+} \\ y_{sk-} \\ y_{0k+} \\ y_{0k-} \end{bmatrix} = \begin{bmatrix} 1 & 0 \\ -1 & 0 \\ 0 & 1 \\ 0 & -1 \end{bmatrix} \begin{bmatrix} t_k \\ n_k \end{bmatrix} \leq \begin{bmatrix} T_y \\ T_y \\ 0 \\ N_y \end{bmatrix}, \tag{6}$$

where T_y and N_y are the tangential strength and the normal strength in tension (while the normal strength in compression is set equal to zero, i.e., $-N_y \leq n_k \leq 0$).

Following classic approaches in plasticity, the contact displacement rates at a no-tension, frictional elastic contact point k are expressed as follows[60]:

$$\Delta u_{tk} = \lambda_{sk+} - \lambda_{sk-} + C_{kt}\Delta t_k \tag{7}$$

$$\Delta u_{nk} = -\mu\lambda_{sk+} - \mu\lambda_{sk-} - \lambda_{ok} + C_{kn}n_k + g_{0k},$$

where $\lambda_{sk+}, \lambda_{sk-},$ and λ_{ok} are the non-negative flow multipliers (i.e., resultant displacement rates) corresponding to positive and negative sliding, respectively, and contact opening; $C_{kt} = 1/k_t, C_{kn} = 1/k_n$, where k_t and k_n are the tangent and normal stiffness at contact points; $\Delta t_k = t_k - t_{0k}$, being t_{0k} the known contact shear force. It is worth noting that Equation (7) is related to an associative flow rule of contact displacement rates, being expressed as a function of the transpose of matrix failure conditions Y_k^T reported in Equation (4). As such, displacement rates at contact points may involve dilatancy, which is related to the components $-\mu\lambda_{sk+}$ and $-\mu\lambda_{sk-}$ in Δu_{nk}. In matrix form, for the whole assemblage, it can be posed:

$$\Delta u = Y\lambda + Cc + g_0, \tag{8}$$

where Δu is the $(2c \times 1)$ vector of contact displacement rates; $\lambda \geq 0$ is the $(3c \times 1)$ vector of flow multipliers; C is the $(2c \times 2c)$ diagonal matrix of contact compliances collecting submatrices $C_k = diag(C_{kt} \ C_{kn})$; g_0 is the vector collecting initial known tangential displacement rates and gaps $[-C_{kt}t_{0k}; g_{0k}]$ at each contact point. Similar conditions hold in the case of the rigid contact formulation if the elastic components of contact displacement rates are omitted. Finally, activation of positive values of flow rates associated with contact failure modes is taken into account considering the following complementarity condition[38]:

$$y^T\lambda = 0. \tag{9}$$

3 | FORMULATION OF THE CONTACT PROBLEMS IN TERMS OF OPTIMIZATION PROBLEMS

The systems of equation governing the elastic no-tension and rigid no-tension contact models correspond to two LCPs, a class of mathematical programming problem, which has been extensively investigated in the past decades.[66,67]

On the basis of the governing Equations (1), (4), (8), and (9), the LCP associated with no-tension elastic contact model can be posed as follows:

$$\begin{bmatrix} \cdot & \cdot & A_0 \\ \cdot & \cdot & -Y^T \\ -A_0^T & Y & C \end{bmatrix}_{n\times n} \begin{bmatrix} \Delta x \\ \lambda \\ c \end{bmatrix}_{n\times 1} + \begin{bmatrix} \cdot \\ y \\ \cdot \end{bmatrix} = \begin{bmatrix} f \\ \cdot \\ -g_0 \end{bmatrix}$$
$$\text{s.t. } y \leq 0 \ \lambda \geq 0 \ y^T\lambda = 0, \tag{10}$$

being $n = 3b+3c+2c$ the number of variables of the LCP problem. The problem in Equation (10) can be uncoupled into two dual quadratic programming problems, corresponding to a force-based and displacement-based optimization scheme. This is a noticeably simplification, which allows very efficient solution algorithms to be used, with low computational costs. The equivalent force–based problem can be written as[60,61]:

$$\max -\frac{1}{2}c^T Cc - g_0^T c$$
$$\text{s.t.} A_0c = f$$
$$y \leq 0, \ y = Y^T c, \tag{11}$$

with the number of variables $n = 2c$ (i.e., the contact forces) and number of constraints $m = 3b+3c$. The dual displacement-based optimization problem is:

$$\min \frac{1}{2}e^T Ke - f^T\Delta x$$
$$\text{s.t.} \Delta u = A_0^T \Delta x$$
$$\Delta u = Y\lambda + e + g_0, \ \lambda \geq 0, \tag{12}$$

where $K = C^{-1}$ and $e = Cc$ is the vector of contact tangential deformations and normal elastic interpenetrations (Figure 2C). The number of unknowns is $n = 3b+2c+3c$ and consists of block centroid displacements, elastic contact deformations, and flow multipliers measured at contact points.

For the no-tension rigid contact model with limited compressive strength, an additional unknown is introduced to the contact problem in Equation (10), that is, the collapse load factor α. External forces (including vertical and horizontal components) are expressed as the sum of dead (i.e., vertical) and live (i.e., lateral) loads multiplied by the load factor α, as follows:

$$f = f_D + \alpha f_L. \tag{13}$$

Under the assumption $f_L^T \Delta x = 1$ to ensure that positive energy has to be dissipated by live loads,[68] the LCP in Equation (10) reduces to:

$$\begin{bmatrix} \cdot & \cdot & -f_L & A_0 \\ \cdot & \cdot & \cdot & -Y^T \\ f_L^T & \cdot & \cdot & \cdot \\ -A_0^T & Y & \cdot & \cdot \end{bmatrix} \begin{bmatrix} \Delta x \\ \lambda \\ \alpha \\ c \end{bmatrix} + \begin{bmatrix} \cdot \\ y \\ \cdot \\ \cdot \end{bmatrix} = \begin{bmatrix} f_D \\ -r \\ 1 \\ -g_0 \end{bmatrix}$$

$$\text{s.t. } y \leq 0 \ \lambda \geq 0 \ y^T \lambda = 0, \tag{14}$$

This skew-symmetric LCP problem is equivalent to the following force-based and displacement-based optimization schemes, corresponding to dual linear programming problems[61]:

$$\begin{aligned} \max \quad & \alpha - g_0^T c \\ \text{s.t.} \quad & A_0 c = f_D + \alpha f_L \\ & y \leq 0, \ y = Y^T c - r, \end{aligned} \tag{15}$$

with the number of static variables $n = 2c+1$ (i.e., contact forces and collapse load multiplier) and number of constraints $m = 3b+3c$;

$$\begin{aligned} \min \quad & r^T \lambda - f_D^T \Delta x \\ \text{s.t.} \quad & f_L^T \Delta x = 1 \\ & \Delta u = A_0^T \Delta x \\ & \Delta u = Y \lambda + g_0, \ \lambda \geq 0. \end{aligned} \tag{16}$$

4 | IMPLEMENTATION

The elastic no-tension and the rigid no-tension contact models are solved on the basis of the solution of optimization problems given in Equations (11), (12), (15), and (16), respectively. More in detail, for a given configuration x_0, the static variables c associated with the prepeak response of the pushover curves corresponding to unilateral elastic contacts are obtained from the solution of problems (11), while the kinematic variables Δx in (12) are directly obtained from the Lagrange multiplier associated with the solution of the same force-based problem. An incremental solution procedure was implemented to consider the effects associated with the change in geometric configuration in the large displacement regime. The procedure involves the updating of equilibrium matrix A and contact gaps vector g at each increment, which are determined on the basis of the new configuration $x = x_0 + \Delta x$. A force control loading numerical protocol is adopted, thus imposing at each step an increasing value of the lateral loads f_L, which in this case are expressed as a known and increasing factor of vertical loads f_D. A similar solution procedure was adopted for the evaluation of the rigid body behavior of the failure mechanism, by solving Equation (15) to derive static variables (now α and c) and Lagrange multipliers associated

with kinematic variables in (16). In this case, it should be noted that the descending branch with decreasing values of α is obtained as direct consequence of the solution of static equilibrium conditions on the deformed structural configuration, as in the case of the postpeak responses obtained from analytical models.

Considering that the model is formulated within a static regime, it should be pointed out that convergence problems of the implemented procedures may occur when a block detaches completely from the rest of the structure, that is, when all the gaps at the potential contact points are open. Equilibrium conditions of the detached blocks should be formulated in the dynamic regime to describe the progressive collapse and this is out of the scope of the present study. In case, a block completely detaches from the rest of the structure, the displacement capacity predicted by the proposed model is dictated by the rocking and sliding behavior of a single block, rather than by the displacement capacity associated with the incipient collapse of the entire failure mechanism.

A MATLAB code was generated to implement the formulation presented for nonlinear elastic and Kinematic Analysis of 2D rigid Block assemblages (KinABlock_2D, https://doi.org/10.5281/zenodo.5018923). The code was organized into a main file and into different functions for: the assignment of input parameters; the generation of the rigid block configuration; the formulation and the solution of the optimization problems corresponding to the formulated contact problems; and the postprocessing of the results. The geometric configuration of the rigid block assemblage can be easily imported from .DXF files, where blocks are modeled using polylines, with vertices corresponding to contact faces. The optimization solver Mosek (ver 9.1.10) was used to solve the corresponding optimization problems. The analyses were carried out using a PC containing a 3.3GHz Intel Xeon E3-1245 processor with 8 GB of RAM.

The numerical parameters, which are needed for the analysis, are: the normal and tangential stiffness k_n and k_t at the contact points, along with the masonry compressive strength and the friction coefficient of the joints. The normal stiffness at each contact point is calculated on the basis of joint stiffness k_{jn}, as follows: $k_n = (k_{jn} \cdot l_j \cdot d_j)/4$, being l_j and d_j the length and the depth at joint j and considering that a four-point contact model was assumed at each interface. The normal joint stiffness is derived from the elastic modulus of masonry according to the expression $k_{jn} = E/h_b$, being h_b the height of the blocks, usually employed to replicate the stiffness of the corresponding continuum element.[53] The tangential stiffness is set as a function of the normal stiffness, after definition of a Poisson ratio for the joint, as detailed in the following examples and according to Ref. 53. When tie elements are used, input parameters include the longitudinal stiffness of the tie, plus its plastic strength and the elongation limit (when strength goes to zero). These parameters are used to define the contact stiffness and strength properties at the end nodes of the tie element.

5 | VERIFICATION BY NUMERICAL EXAMPLES

A series of numerical benchmarks were performed to evaluate the accuracy of the proposed modeling approach in the derivation of the pushover curve for masonry panels subjected to lateral seismic actions. The benchmarks comprise hand-calculations resulting from the application of the virtual work principle in the large displacement regime (nonlinear kinematic analysis), closed-form solutions from the literature, and distinct element simulations.

5.1 | Side wall and facade connected by a tie rod

The behavior of a system of two blocks connected by a tie rod, one representing a side wall and one representing a masonry façade subjected to out-of-plane loading, was investigated (Figure 4A). The length of the side wall was $B_1 = 4.50$ m, while the dimensions of the out-of-plane loaded façade was $B_2 = 0.50$ m and $H = 3.50$ m. The blocks were subjected to dead loads P_1 and P_2 equal to 350 and 100 kN, respectively. The façade was loaded by a varying lateral load αP_2. The friction coefficient μ and the compressive strength f_c of the masonry were set equal to 0.6 and 1.0 MPa, respectively, while the joint stiffness k_{jn} was 1.0e5 kN/m³. No contact was defined for the interface between the side wall and the façade. The tie was positioned at a distance c of 0.25 m from the top, had a stiffness of 500.0 kN/m, and a yielding force of 5.0 kN. The ductility of the tie rod was considered by setting an elongation threshold of 0.20 m (strain of 4%). The bases B_1 and B_2 were first discretized into 8 and 1 contact interfaces, respectively.

Figure 5A shows the pushover curves obtained with the rigid body model when using the default four-point contact discretization. Results are shown both for the free standing and strengthened façade, and when infinite and limited compressive strength, that is, rocking and crushing behavior, are considered. A good agreement is observed with the hand-calculations derived from simple equilibrium conditions on the original and varied configurations (Table 1). For the façade
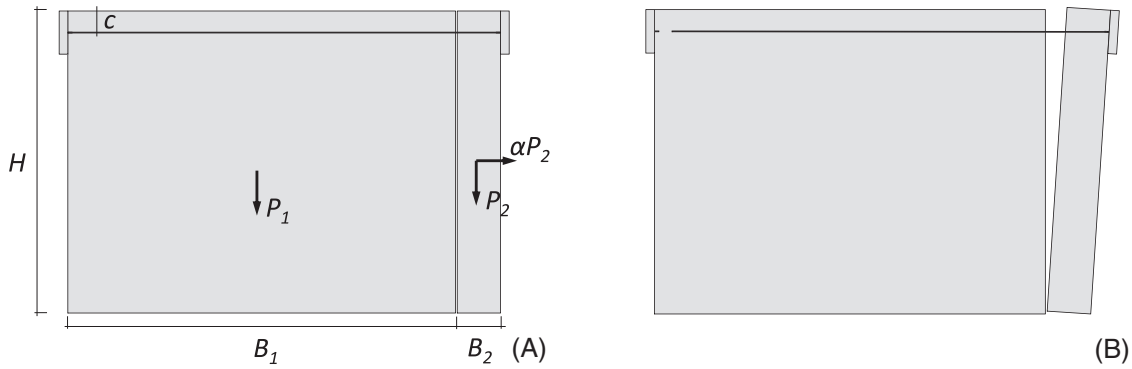
FIGURE 4 Modeling of a side wall and façade connected by a tie rod: (A) Configuration and load distribution in the two panels. (B) Overturning failure mechanism of the facade
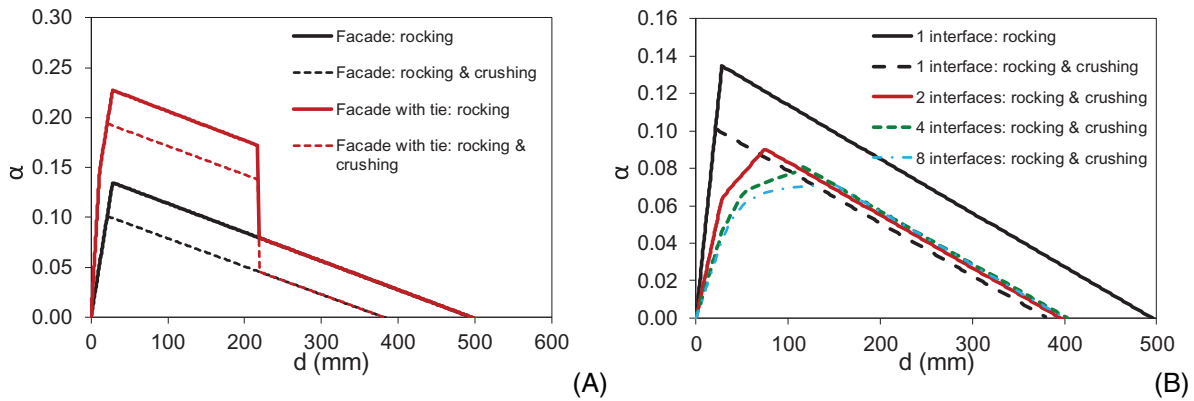

FIGURE 5 Modeling of a side wall and façade connected by a tie rod: (A) Pushover curves for the out-of-plane failure mechanism of the facade, with rocking and crushing behavior, without and with tie rod, when its base B_2 is discretized with a single contact interface. (B) Sensitivity analysis to the number of contact interfaces at the base without tie

with the tie rod, a stiffness change can be noted in the elastic response, corresponding to the opening at one vertex of the base contact interface. It can be also noticed that the pushover curves of the strengthened façade, both for infinite and limited compressive strength, fall on the ones of the free-standing façade when the elongation limit is exceeded in the tie rod. This type of discontinuities in the pushover curve are treated without convergence problems by the model. This is a direct consequence of the solution procedure adopted here, according to which, when reaching the ductility limit of the tie element, zero strength is set for the tie in the failure conditions of Equation (5).

Figure 5B shows the results of the sensitivity analysis carried out on the number of contact interfaces at the base of the facade, which was varied from 1 to 8, corresponding to 4 and 32 contact points. As expected, the pushover curves are remarkably influenced by the number of contact points for what concerns the elastic response and in particular the initial stiffness K. Conversely, the load multiplier α_0 and the displacement capacity d_0 are only slightly affected when crushing

TABLE 1 Modeling of a side wall and façade connected by a tie rod: comparison between analytical and numerical results when a single contact interface is used at the base of the overturning facade

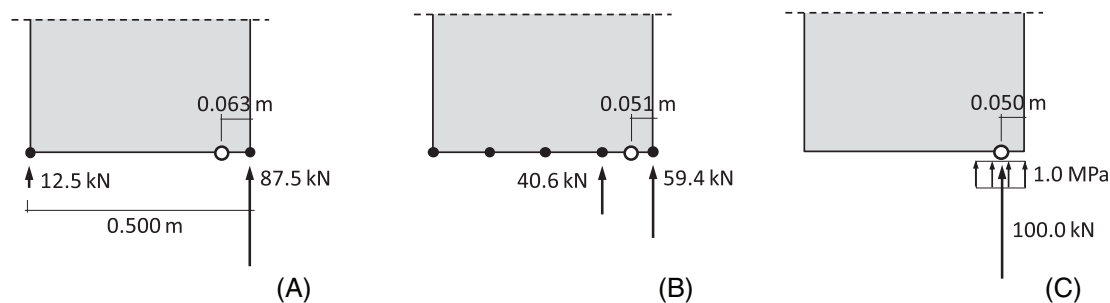|		Analytical						Proposed					
		Elastic	Rocking		Crushing			Elastic	Rocking		Crushing		
Case study	Model size ($b \times c$)	K(N/mm)	α_0	d_0(mm)	α_0	d_0(mm)		K(N/mm)	α_0	d_0(mm)	α_0	d_0(mm)	
Two wall panels w/o tie	2×36	489	0.143	495	0.114	397[a]		497	0.143	493	0.107	379	
Two wall panels with tie	5×60	1344	0.236	495[a]	0.207	397[a]		1347	0.236	493[a]	0.200	379[a]	

[a]With tie elongation threshold.

FIGURE 6 Modeling of a side wall and façade connected by a tie rod. Distribution of resultant contact forces for crushing and position of rotation center at the base of the overturning facade in the case of: (A) one contact interface; (B) four contact interfaces, and (C) stress-block assumption

is modeled, as a consequence of the underlying failure conditions adopted, which are expressed at the level of the entire interface as a function of stress resultants.

For the case of rigid contacts with crushing, a comparison between the contact forces calculated for an increasing number of interfaces and the distribution of stresses corresponding to the stress-block solution is reported in Figure 6. The position of the center of rotations, corresponding to the line of action of the resultant of contact forces, is also reported (Figure 6A, B). The comparison with the analytical solution (Figure 6C) shows that the positions closely match for a number of contact interfaces equal to 4.

5.2 | Dry-stacked masonry panels with openings

The accuracy of the rigid block model was further evaluated by comparing its response with numerical simulations performed by the distinct elements method (DEM). The dry-stacked masonry panels originally proposed by Baggio and Trovalusci[69] and later revisited by Ferris and Tin-Loi[38] and Gilbert et al.[39] were used as a benchmark. The panels were modeled by means of the software package UDEC 6.0.[51] The ability of UDEC to model the out-of-plane rocking behavior of masonry structures is demonstrated in earlier works, see, for instance, Refs. 26, 28, and 70. In this study, UDEC was used to create a numerical mock-up of the panels with the same geometry and material properties as those used in the rigid block model.

The panels originally consist of building blocks of nondimensional length 4.0, height 1.75, and mass density equal to 1.0.[38] For the purpose of the present study, full block dimensions were set equal to 0.4×0.175 m and a unit weigh of 10.0 kN/m³ was assumed. Differently from the original benchmarks, the block corners were rounded by a radius of 0.02 m. It can be noticed that this is a default parameter to be taken into account when using UDEC 6.0.[51] The default two-point contact discretization was used between adjacent blocks, in both the DEM and rigid block models. A Coulomb slip contact model with integration over the contact area was adopted for the joints of the DEM model.[51] More particularly, in order to mimic the contact behavior of the rigid body model, contact was modeled as elastic-brittle under tensile loading, elastic under compressive loading, and elastic-perfectly plastic under shear loading. In the original works,[38,39] all joints had zero cohesion, zero tensile strength, and the same frictional behavior (associative and nonassociative) with friction angle of 33°. To test the applicability of the rigid block model under various configurations, in this benchmark, the bed joints had associative behavior with friction angle of 33°, while the head joints were assigned zero friction angle. The normal joint stiffness was set equal to 1.0e5 kN/m³ and the shear stiffness was derived by using a Poisson's ratio of 0.2.

The panels were supported on a rigid foundation and the properties of the base joints were the same as those used for the bed joints. All blocks were subjected to the self-weight f_D plus a horizontal live load αf_L simulating the seismic loading. A solution strategy conceptually similar to the relaxation method and making use of local damping was implemented in UDEC to ensure quasi-static loading conditions throughout the analysis and, more specifically, the correct representation of the postpeak behavior of the pushover curves.[8] Differently from the rigid block model, the DEM model makes use of an explicit time integration scheme. Calculations are organized into cycles, where Newton's second law of motion is solved for all blocks, and stress-displacement laws derive contact forces from the known displacements to be used in the

equations of motion. With this solution scheme, mechanical damping is needed to obtain the static solution and prevent, or reduce, oscillations.[51]

Figure 7 shows the pushover curves and the related collapse mechanisms obtained by the models. The load multiplier α versus the displacement d extracted at top right corner of each panel is plotted. Both the rigid and the elastic versions of the rigid body model are presented. The plots of the collapse mechanisms are extracted for both the rigid block and DEM model at $d = 200$ mm.

In all examples, the pushover curves provided by the rigid block model compare fairly well with the DEM model in the prepeak behavior. This is less evident only in Examples 1 and 2, where shear elastic deformations play an important role as compared to the other examples. Moreover, in all examples, the descending curve obtained by the rigid block model follows closely the slope of the postpeak behavior of the DEM model. Finally, the peak multiplier provided by the rigid block model, found at the interception between the "elastic" and the "rigid" curves, compares well with the peak multiplier predicted by the DEM model. The displacement capacity of the structure, which in the rigid block model corresponds to the point where the algorithm fails to predict the solution, occurring when one block detaches from the rest of the structure, compares well to the points where abrupt changes in the response are observed in the DEM solution.

Concerning the collapse mechanisms predicted by the models, the comparison is also satisfying for most examples, in that the blocks that are mobilized in the mechanisms are similar. Differences in the failure modes can be noted for Examples 2 and 3, which can be also ascribed to the different solution strategies adopted for the postpeak behavior. For the proposed rigid block model, apparent nondilatant behavior occurs at joints when sliding, despite the assumed associative flow rule (Equation 8). In particular, the equations governing the kinematic rules involve a dilatant behavior at sliding joints only in the initial increments of the sequential solution procedure. The new gaps created by the associative sliding behavior of the first increments tend to cancel out the dilation in the next increments, thus resulting in an apparent nondilatant behavior. A detailed discussion on this aspect related to assumed associated sliding rule, which was also observed in Ref. 35, is given in Ref. 59.

6 | COMPARISONS WITH EXPERIMENTAL TESTS

In this section, applications to experimental case studies, both developed for the present study and from the literature, are considered to evaluate the accuracy and computational efficiency of the developed formulations when multiblock assemblages are considered. Experimental tests, including also the effects of strengthening with ties, are considered.

6.1 | Dry joint stone shear walls

The dry stone masonry shear walls SW.30 tested by Lourenço et al.[53] were considered for comparison (Figure 8). The dimensions of the stone walls were 1000×1000×200 mm and the size of the units was 100×200×200 mm. The walls were subjected to a precompression vertical load of 30.0 kN and to a varying horizontal load at the top. The mechanical properties of the rigid block model were set in accordance to the values reported in Lourenço et al.[53] and Orduña and Lourenço.[71] A unit weight of 25.0 kN/m^3 was considered for the rigid blocks. The values considered by these authors were adopted for the friction coefficient, 0.66, and the normal joint stiffness k_{jn}, 5.66e6 kN/m^3. The tangential stiffness was set equal to $k_{jt} = k_{jn}/(2(1 + 0.2))$, being 0.2 the value assumed for the Poisson's ratio, according to Ref. 53.

The predicted failure mechanism is shown in Figure 8A and corresponds to simple overturning, with a diagonal stepped crack propagating from the left end corner at the base. The comparison with experimental outcomes shows a good agreement with numerical response in terms of pushover curves (Figure 8B). The failure modes observed from experimental tests were also very similar to that predicted with the proposed model. Experimental failure occurred by a simple rotation of the upper part of the wall with a stepped diagonal crack propagating along the bed and head joints from the half block at the bottom left end side of the wall panel. Sliding along the bed joints was also observed.[53]

6.2 | Dry joint stone portal frame

The capability of the developed formulation in predicting the failure modes and the lateral force for the onset of the collapse mechanism with tie elements is tested by comparing it with the results of tilting tests carried out on a dry jointed
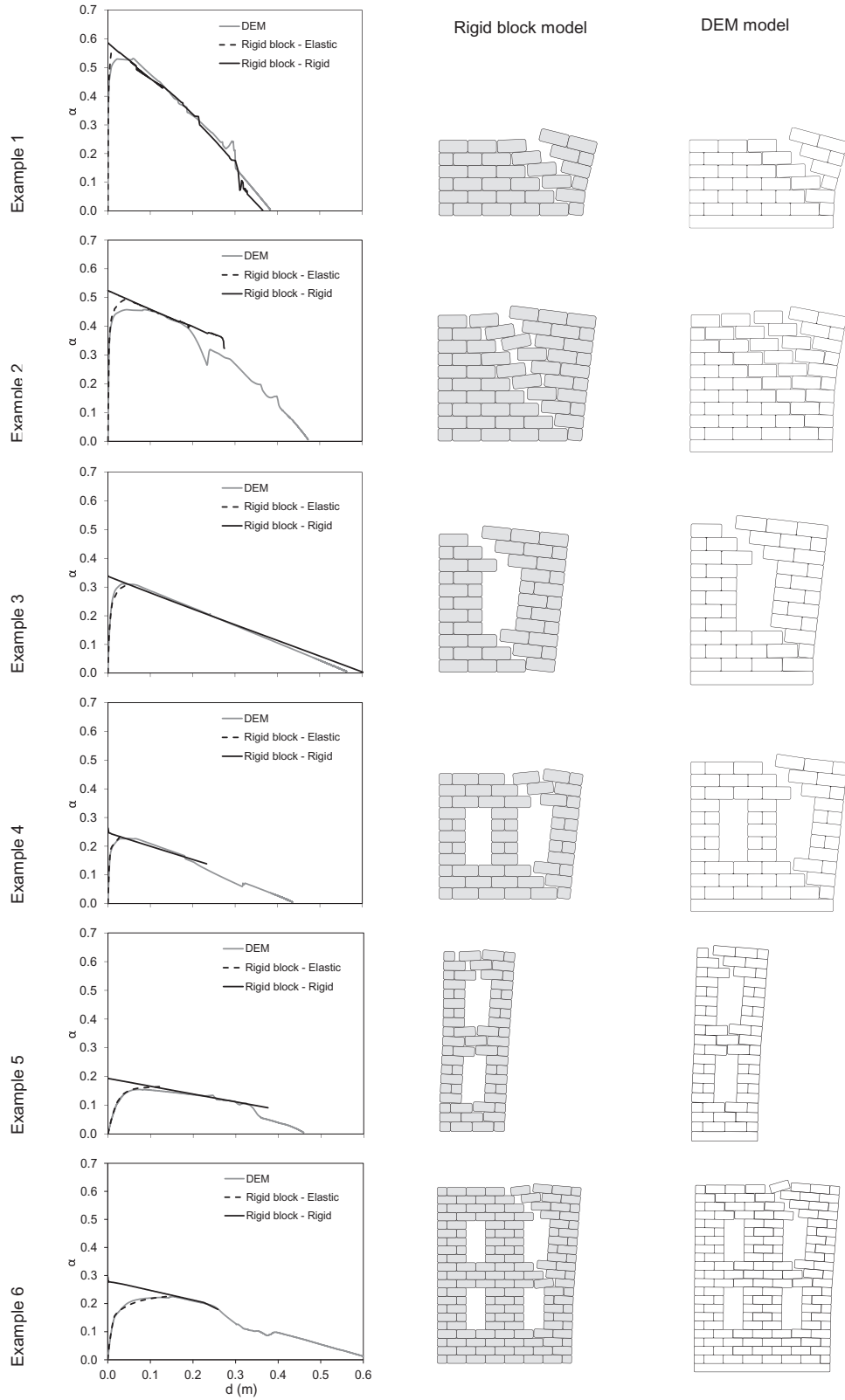
FIGURE 7 Modeling of dry-staked masonry panels with openings: comparison of the results of the proposed model with DEM simulations
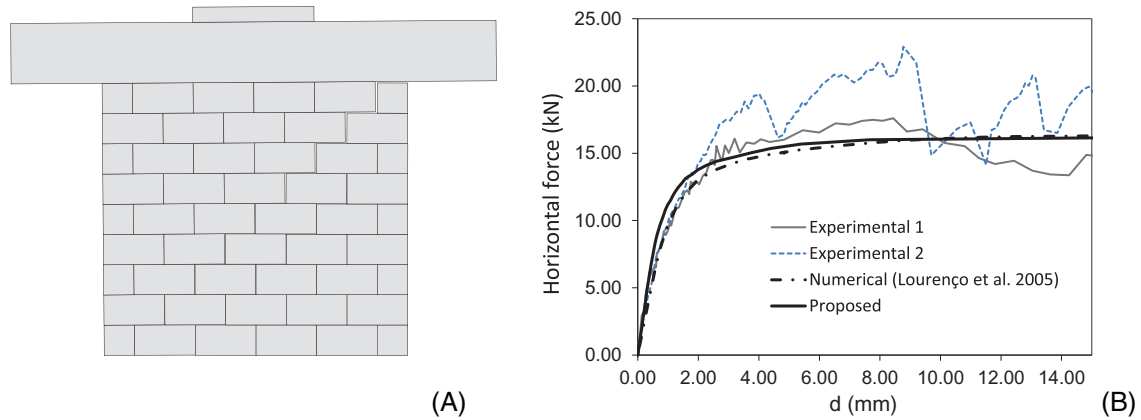
FIGURE 8 Analysis of the SW.30 wall panels[53]: (A) deformed configuration and (B) comparison of with the experimental curves
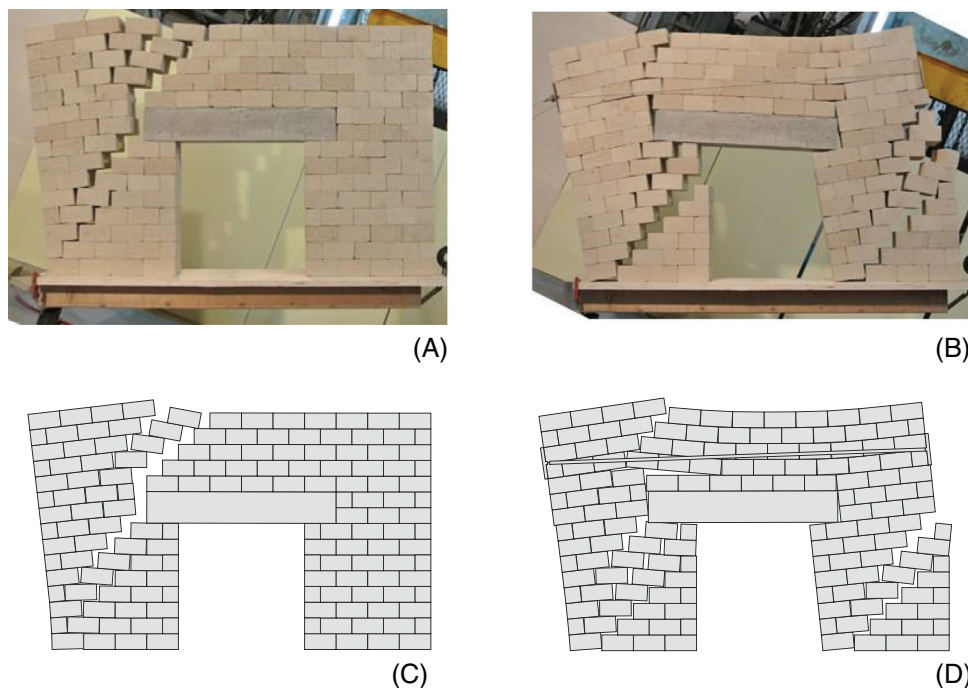

FIGURE 9 Dry joint wall panels: comparison of experimental and numerical failure mechanisms for free (A and C) and reinforced configurations (B and D)

masonry panel with an opening. The blocks were made of tuff stones with size 100×100×50 mm. A lintel 600×100×100 mm made of reinforced cement mortar was used to span the opening. The unit weights of the tuff stones and the reinforced cement beam were 12.1 and 14.0 kN/m^3, respectively.

The test set up was similar to the one used by Portioli et al.[72] The tilting table was made of a timber beam hinged at one end and was lifted up by a chain puller, so to induce the collapse by progressively increasing lateral forces as a function of blocks self-weight and tilting angle. The average value of the friction coefficient measured from sliding tests on the tilting table on two blocks stacks was 0.51. The tie was a steel wire cable with diameter of 1.0 mm, which was connected to two steel plates with dimensions 100.0×100.0×3.0 mm. The tie plastic strength used for numerical simulations was set equal to 100.0 N.

The failure mechanisms and the values of lateral load multipliers obtained from experimental tests and the rigid block model for the onset of motion are shown in Figure 9 and Table 2. A good agreement in terms of failure modes can be noted, whereas the load factors for the onset of motion are slightly overestimated in this case, with differences up to about 12.8% for the free-standing configuration. These differences are likely due to the geometrical irregularities of the tuff blocks.

TABLE 2 Numerical and experimental wall panels with tie: collapse load multiplier and CPU times

| | Model size | Block model with rigid contacts | | Experimental |
Case study	$(b \times c)$	α_0	CPU time[a] (s)	α_{exp}
Exp. wall panel w/o tie	149×1612	0.44	0.56	0.39
Exp. wall panel with tie	152×1636	0.50	0.58	0.49

[a]CPU time per displacement increment, referred to 3.3GHz CPU.
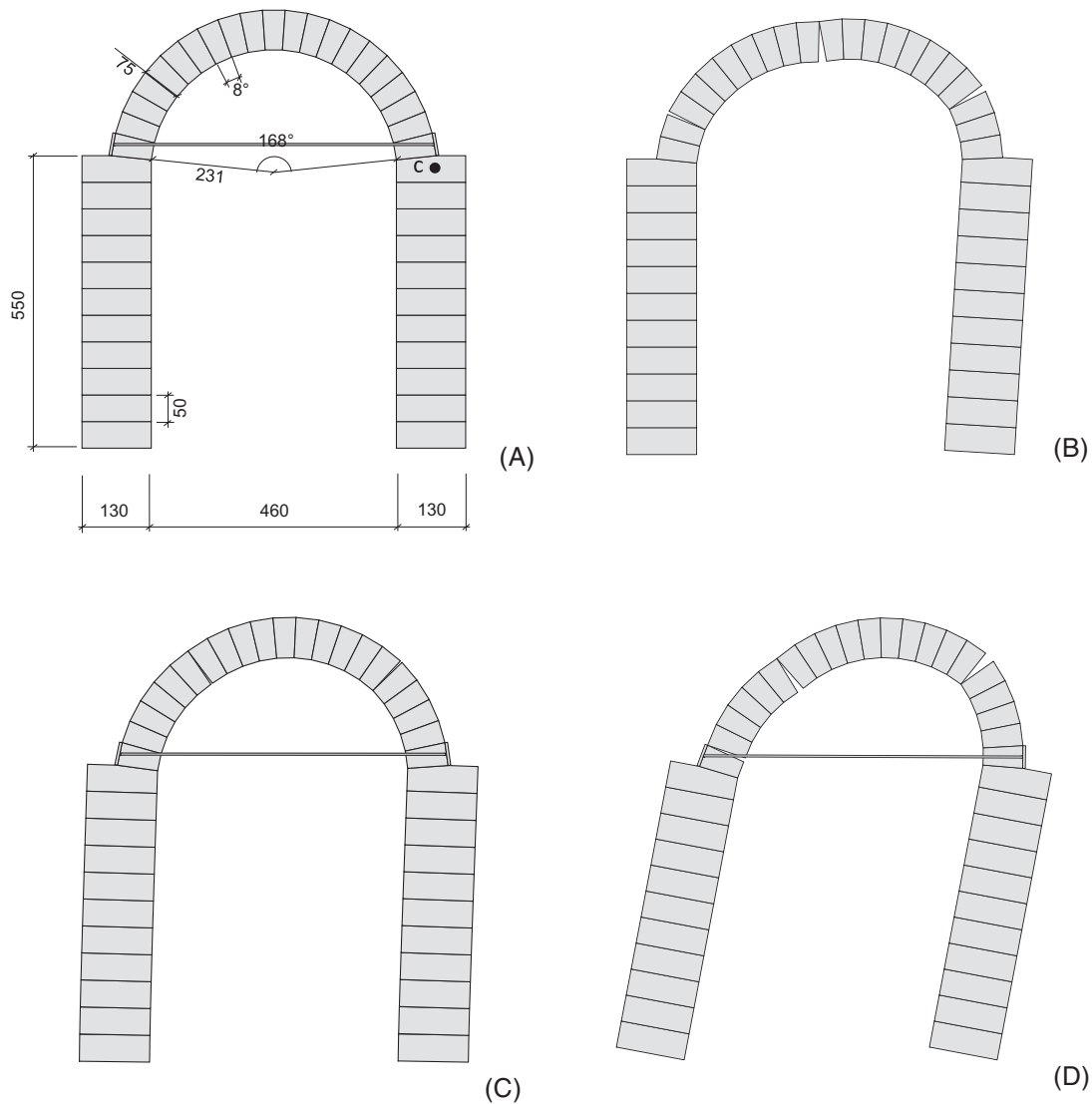

FIGURE 10 Modeling of a buttressed arch with tie: (A) geometry; (B) failure mechanism of the free block model with rigid contacts, and (D) with tie; (C) deformed configuration of the block model with elastic contacts and tie

6.3 | Dry-stacked buttressed arches

The buttressed arches experimentally investigated in Calderini and Lagomarsino[52] were considered for comparison. The specimens were made of dry-jointed plastic blocks with polyvinyl alcohol tissues at interfaces to increase the friction coefficient and prevent sliding. The buttressed arches were tested on a tilting table and block displacements were recorded using a 3D motion capture system. Two different configurations were considered, namely, the free-standing buttressed arch and the buttressed arch reinforced with a tie rod.

The dimensions of the buttressed arches and the configuration of the rigid block model are shown in Figure 10A. The value of the unit weight of the blocks was set equal to 11.5 kN/m^3 and the friction coefficient was taken to be 0.6, in
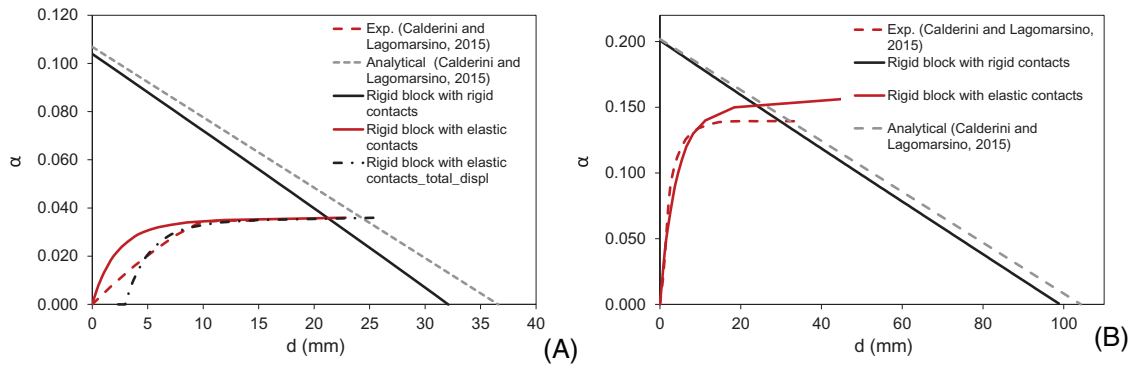
FIGURE 11 Buttressed arches: comparison of experimental, analytical, and numerical pushover curves without (A) and with tie element (B)

accordance with Calderini et al.[11] and Calderini and Lagomarsino.[52] The normal joint stiffness at block interfaces was set equal to 1.2e5 kN/m³, considering the elastic modulus, which was measured for the blocks and tissues at the interfaces (which were equal to 1800 and 0.06 MPa, respectively), and corresponding dimensions. The longitudinal stiffness of the tie rod made of a guitar string made of harmonic steel was set equal to 4.9 kN/m, corresponding to a circular tie rod with length 430 mm, an elastic modulus of 67,000 MPa, and a nominal diameter of 0.2 mm. The tie strength and the elongation threshold were set equal to 88.0 N and 20.0 mm (strain of 4.6%), respectively, according to Ref. 52. The failure mechanism corresponding to the rigid contact formulation without and with tie element is reported in Figure 10B, D. In Figure 10C, the deformed configuration obtained in the case of elastic contacts with tie is also shown.

The comparisons of numerical pushover curves with analytical and experimental curves presented in Ref. 52 are reported in Figure 11. In the case of the specimen without tie rod, Figure 11A shows the elastic pushover curves corresponding to the total lateral displacement at the control point, that is, the lateral displacement which includes the effects of self-weight and horizontal loads, and the lateral displacement corresponding to horizontal loads only (i.e., the lateral displacement for vertical and lateral loads *minus* the lateral displacement for vertical loads). According to the experimental results, the analysis on the free-standing block model shows that the deformation of the joints (and the large displacement formulation) reduces the force capacity of the system considerably. A good agreement with experimental test in terms of failure load is observed. Conversely, remarkable differences in the prepeak, elastic response can be noted. Those could be ascribed to geometric imperfections, that is, global misalignments and local imperfections, such as rounded corners of the blocks observed during the tests[52] and to the simple point contact model adopted. Similar differences can be noted in the case of the buttressed arch with tie, although in this case a slight difference in the predicted collapse load is also observed.

7 │ SEISMIC ASSESSMENT OF A TRIUMPHAL ARCH

The prototype of a triumphal arch was considered to test the suitability of the proposed modeling approach for the seismic assessment procedures contained in the Italian technical standard for local collapse mechanisms of masonry structures.[3,4]

The dimensions of the triumphal arch are reported in Figure 12A. The depth of the circular arch was set equal to 0.60 m and that of the nave walls was 5.50 m, the latter corresponding to the distance between two consecutive triumphal arches. The size of the masonry units in the piers was 0.40 × 0.30 m. The unit weight of masonry was 16.0 kN/m³ and the friction coefficient was set equal to 0.65. The normal joint stiffness was 5.3e6 kN/m³, so to replicate the elastic behavior of the continuum corresponding to a Young modulus E of 1600 N/mm² for a block height of 300 mm. The compressive strength was 1.00 MPa. Additional vertical loads equal to 100.0 kN were considered at the top of the nave walls to simulate the action induced by the roof. Two different values for the tie strength, 10.0 and 50.0 kN, were considered to investigate the influence of strengthening interventions on the failure mechanisms and seismic capacity of the arch. The longitudinal stiffness of the tie was set equal to 1850 kN/m, corresponding to a wire rod with an equivalent elastic modulus and cross-section of 110,000 MPa and 123.5 mm², respectively. The elongation threshold in the tie was 74 mm, corresponding to a limit plastic strain of 1%. Concerning the contact discretization, bed joints between full blocks in the piers were divided into two contact interfaces, whereas a single contact interface was used for the head joints. The joints between the arch voussoirs
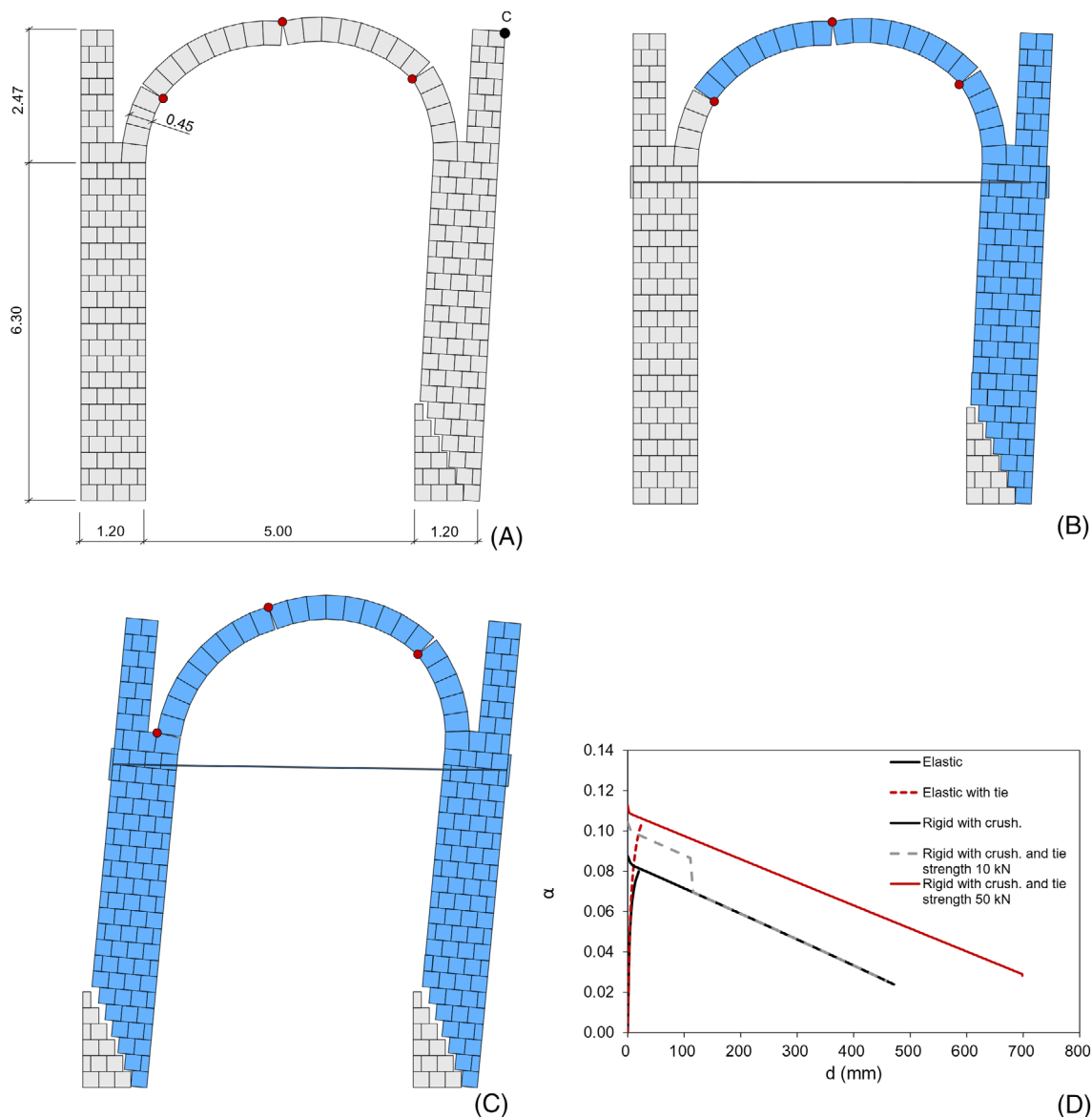
FIGURE 12 Seismic assessment of a triumphal arch: failure mechanisms and mobilized blocks (in blue color) obtained from the rigid contact formulation without tie (A), with tie strength equal to 10.0 kN (B) and equal to 50.0 kN (C). Pushover curves (D)

were divided into four contact interfaces. As observed in Section 5.1, a configuration with four contact interfaces allows for the correct representation of the stress block distribution and the position of the pivot point between two adjacent blocks.

The collapse mechanisms obtained from the analyses are shown in Figures 12A–C. The mechanisms predicted for the unstrengthened arch and arch strengthened with tie of strength equal to 10.0 kN are similar, with the overturning of a single wall and the formation of three hinges in the circular arch. The analysis also shows that the tie strength of 10.0 kN is attained and a visible plastic elongation occurs. Conversely, for the tie with strength equal to 50.0 kN, the failure mechanism involves the overturning of both walls, while the tie does not fail and acts as a rigid link between them.

The pushover curves predicted by the model are shown in Figure 12D. The control point C was selected at the top of the right end pier. For the buttressed arch with the tie strength equal to 10.0 kN, a remarkable increase is observed with respect to the unstrengthened arch in the force capacity α_y, while low is the difference in terms of elastic displacement, d_y. After reaching the force capacity, the failure load multiplier is still high, up to the attainment of the plastic threshold in the tie, occurring at about 120 mm, after which the pushover curve falls on the one of the unstrengthened arch. Finally, the displacement capacity d_0 of the unstrengthened arch and the arch strengthened with tie of strength equal to 10.0 kN is the same. For the arch strengthened with tie of strength equal to 50.0 kN, a larger value is observed for both the force and displacement capacities. This can be ascribed to the different positions and movement of the hinges in the circular
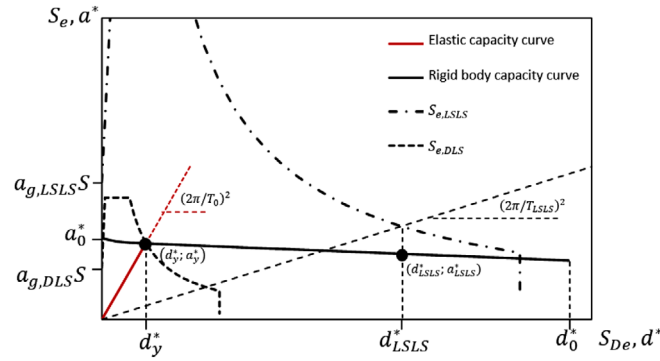
FIGURE 13 Seismic assessment of a triumphal arch: implementation of the force- and displacement-based seismic assessment methods contained in the Italian Technical Standard[3,4] by means of the proposed rigid body model

TABLE 3 Seismic assessment of a triumphal arch: parameters obtained from numerical simulations for pushover and capacity curves

		Triumphal arch w/o tie	Triumphal arch with tie strength 10.0 kN	Triumphal arch with tie strength 50.0 kN
Model size ($b \times c$)		253×2720	256×2744	256×2744
α_0		0.088	0.104	0.113
α_y		0.080	0.100	0.105
d_y (mm)		19	20	26
d_0 (mm)		471	471	698
e^*		0.790	0.791	0.792
Γ^*		0.670	0.671	0.680
$a_0^*(d^* = 0)$ (g)		0.082	0.098	0.106
d_0^* (mm)		316	316	475
T_0 (s)		0.83	0.76	0.86
T_{LSLS} (s)		2.52	2.52	2.77
$\zeta_{E,DLS}$	Force-based	0.66	0.78	0.85
	Displ.-based	0.54	0.60	0.73
$\zeta_{E,LSLS}$	Force-based	0.52	0.62	0.67
	Displ.-based	0.66	0.66	0.94

arch, which govern in all cases the capacity of the structure. From a practical point of view, it confirms the use of a tie rod of 50.0 kN as a possible seismic retrofitting solution.

The capacity curves of the equivalent SDOF system were derived from the pushover curves obtained with the rigid block model, by using appropriate transformation factors (Figure 13). According to Ref. 3, the spectral acceleration is defined as $a^* = \frac{\alpha(d_C)}{e^* CF} g$, where $e^* = \frac{(\sum P_i \delta_{x,i})^2}{\sum P_i \sum (P_i \delta_{x,i}^2)}$, while the spectral displacement is $d^* = d_C \Gamma^*$, where $\Gamma^* = \frac{\sum P_i \delta_{x,i}^2}{\delta_{x,C} \sum P_i \delta_{x,i}}$. In the equations, e^* is the ratio of participating mass, CF is the confidence factor, d_C is the displacement of the control point, Γ^* is the spectral transformation factor for displacements, and $\delta_{x,i}$ are the horizontal displacements. A routine was implemented for the automatic calculation of the factors e^* and Γ^* by the rigid block model. The parameters characterizing the pushover and capacity curves are reported in Table 3. The displacement d_y and the initial period $T_0 = 2\pi \sqrt{\frac{d_y^*}{a_y^*}}$ are referred to the intersection point between the initial branch and the descending curve of the rigid body model. In the calculations, a confidence factor CF of 1.35 was used.

The seismic safety assessment was carried out according to the force-based and displacement-based methods for the damage and life-safety limit states, indicated, respectively, as DLS and LSLS. The following parameters were considered for the seismic demand at LSLS, corresponding to the site of L'Aquila, Italy: $a_g = 0.261g$; $F_0 = 2.364$; $T_C^* = 0.347s$, being a_g the design peak ground acceleration on stiff soil, F_0 the amplification factor, and T_C^* the reference value for the determination of the natural period corresponding to the constant velocity spectrum region. At DLS, the considered spectrum parameters

were: $a_g = 0.104g$; $F_0 = 2.332$; $T_C^* = 0.281s$. A soil factor $S = 1.2$ was assumed for both DLS and LSLS, corresponding to a soil of type B. The viscous damping ratio ξ used in for the calculation of the spectra was set equal to 5% and 8% for DLS and LSLS, respectively.[3,4]

Applying the force-based method, a rigid behavior was assumed up to the activation of the failure mechanism. In this case, the peak ground acceleration that corresponds to the activation of the failure mechanism at DLS was evaluated as follows[3]: $a_{g,DLS} \cong \frac{a_0^*}{S}$, being $a_0^* = a^*(0)$. The peak ground acceleration corresponding to LSLS was calculated by applying a behavior factor $q = 2.0$ to the expression above.[3]

For the application of the displacement-based method, the spectral displacement capacities corresponding to DLS and LSLS were d_y^* and d_{LSLS}^*, with $d_{LSLS}^* = 0.4d_0^*$. The equivalent period corresponding to d_{DLS}^* was T_0, while the one corresponding to d_{SLS}^* was $T_{LSLS} = 1.68\pi\sqrt{\frac{d_{LSLS}^*}{a_{LSLS}^*}}$.[3] The peak ground acceleration capacity $a_{g,LS}$ at a given limit state LS was evaluated from the corresponding spectral acceleration capacity $S_{e,LS}$, through the relationship: $d_{LS}^* = S_{e,LS}(T_{LS})\frac{T_{LS}^2}{4\pi^2}$, where d_{LS}^* is the spectral displacement capacity corresponding to DLS or LSLS, that is, d_y^* or d_{LSLS}^*, and T_{LS} is the corresponding period, that is, T_0 or T_{LSLS}.

In Table 3, the safety indexes ζ_E, which express the ratio between the capacity and demand peak ground accelerations $a_{g,LS}$ and a_g, are reported both for the force- and displacement-based methods. In general, for all studied configurations, at DLS the displacement-based method provides lower indexes with respect to the force-based method, with differences up to about 20%. Several authors have reported a similar difference between the force capacity obtained from experimental tests on unreinforced masonry walls and the one obtained by rigid body kinematic analysis, see Ref. 57.

Conversely, larger indexes are obtained by application of the displacement-based method at LSLS, which can be ascribed to the large displacement capacities observed for the arch. Comparing the three structural configurations considered, the difference between the obtained safety indexes is remarkable and up to about 40% for the tie of strength 50 kN.

8 | CONCLUSIONS

A rigid block model with no-tension, frictional, and crushing contact interfaces was presented in this study for the nonlinear pushover analysis of historic masonry structures. The model relies on two kinds of behavior at contact interfaces to capture the pre and postpeak responses corresponding to the initial elastic behavior and to the mechanism activation and rocking behavior under lateral loads.

The potential for using the proposed model to assess and design masonry structures when subjected to earthquakes according to the methods contained in the technical standards has been shown in this paper by a series of analytical and numerical benchmarks, along with comparisons against experimental tests and an application to the seismic assessment and strengthening of a triumphal arch.

The comparisons showed that the numerical results closely match those of the corresponding solutions. This outcome confirms the suitability of the modeling strategy adopted here, which strictly complies with the analytical models recommended in standards, where the failure mechanism is schematized into a system of rigid bodies separated by no-tension interfaces, whose behavior is governed by the equilibrium conditions, which can be derived from the application of the virtual work principle. Sensitivity analysis showed that the elastic response and force capacity are remarkably affected by the number of contact points used on the block interface. This may have a large influence when a macromodeling approach is attempted, that is, when a single block is adopted to represent an entire structural element. Conversely, the number of contact points only slightly influences the postpeak response and displacement capacity of the structure obtained from the rigid contact formulation. This is due to the formulation of the failure conditions adopted for crushing, which is defined on the basis of force resultants at contact points and on the basis of the failure domain corresponding to the classic stress-block assumption.

Comparisons with distinct element solutions on classic benchmarks inspired by limit analysis also showed a good agreement for the proposed model, both in terms of failure mechanisms and pushover curves. In few cases, it was observed that the displacement capacity computed by the rigid block model is lower than that obtained from distinct element modeling. This is due to slight differences in the obtained failure mechanisms, which in the case of rigid block model also involve the sliding of single blocks upon the contact surfaces of the bottom block. As such, the displacement capacity in the failure mechanism obtained from the rigid block model corresponds in these cases to the loss of contact between adjacent blocks, rather than to the loss of equilibrium stability of the entire failure mechanism.

Applications to experimental tests also showed that the element which was developed for ties provides reasonably accurate and reliable assessment of the structural behavior when strengthening interventions are considered.

Finally, the seismic assessment of a triumphal arch performed according to codified procedures showed that the parameters of the capacity curve, which are related to the failure modes and the participating mass of the blocks involved in the mechanism, can be easily obtained with the implemented model, thus encouraging its use in practical applications. The differences estimated in this case between safety indexes for the force- and displacement-based method were up to about 20% and 40%, respectively. However, the comparisons between force- and displacement-based methods contained in the new version of the Italian technical standard[3,4] and, more importantly, the evaluation of their consistency with time-history analyses of multiblock assemblages deserve further investigation and should be addressed in future studies. The failure of the masonry units, which was not comprised in the proposed modeling approach, could also be included by formulating internal cohesive interfaces for the blocks, after proper modifications of corresponding failure conditions.

NOMENCLATURE

α	live load multiplier
α_0	load multiplier at the onset of the mechanism with rigid contacts
α_y	load multiplier at the force capacity with elastic contacts
Γ^*	transformation factor for spectral displacements
$\lambda_{sk+}, \lambda_{sk-}, \lambda_{ok}$	flow multipliers for positive, negative sliding and opening at contact point k
$\boldsymbol{\lambda}$	vector of flow multipliers
μ	friction coefficient
$\zeta_{E,DLS}, \zeta_{E,LSLS}$	safety indexes in terms of peak ground accelerations at damage and life-safety limit states
a_0^*	spectral acceleration at the onset of failure mechanisms
$\boldsymbol{A_0}$	equilibrium matrix
b	number of blocks
c	number of contact points
$\boldsymbol{c_k}, \boldsymbol{c}$	vectors of contact forces at point k and at all contact points
$C_{kn}, C_{kt}, \boldsymbol{C}$	normal, tangential contact compliance, and matrix of contact compliances
d, d_y, d_0	displacement of a control point, displacement at the elastic limit, and displacement capacity
$d^*, d_{DLS}^*, d_{LSLS}^*$	spectral displacement, spectral displacements at damage and life-safety limit states
d_j	depth of contact joint j
e_k	normal elastic interpenetrations at contact point k
$\boldsymbol{e}$	vector of tangential elastic deformations and normal elastic interpenetrations at contact points
e^*	ratio of participating mass
$f_{xi}, f_{zi}, f_{\omega i}$	external load components at centroid of block i
$\boldsymbol{f}, \boldsymbol{f_D}, \boldsymbol{f_L}$	vectors of external loads, dead (vertical) and live (lateral) loads
g_{0k}	initial known contact gap at contact point k
$\boldsymbol{g_0}$	vector collecting initial known tangential displacement rates and gaps
$\boldsymbol{K}$	matrix of contact stiffnesses
k_n, k_t	normal and tangential stiffness at contact points
k_{jn}, k_{jt}	normal and tangential stiffness at joints
l_j	length of contact joint j
M_j, N_j	bending and normal force resultants at contact joint j
n_k, t_k, t_{0k}	normal, tangential contact forces and initial known tangential force at contact point k
$\boldsymbol{r}$	vector of constant terms associated with failure conditions
T_0, T_{LSLS}	equivalent periods corresponding to d_{DLS}^* and d_{LSLS}^*
$\boldsymbol{x_0}, \boldsymbol{x}$	vectors of initial (known) and new (unknown) positions at block centroids
y_{sk+}, y_{sk-}, y_{0k}	failure conditions for positive, negative sliding and opening at contact point k
$\boldsymbol{y_k}, \boldsymbol{y}$	vectors of failure conditions at contact point k and at all contact points
$\boldsymbol{Y_k}, \boldsymbol{Y}$	flow rule matrices at contact point k and at all contact points
$\Delta u_{nk}, \Delta u_{tk}$	normal and tangential relative displacements at contact point k
$\boldsymbol{\Delta u}$	vector of local relative displacements at contact points
$\Delta x_i, \Delta z_i, \Delta \omega_i$	displacements at centroid of block i
$\boldsymbol{\Delta x}$	vector of displacements at block centroids

REPRODUCIBILITY OF THE ARTICLE'S CONTENT

ORCID
Francesco P. A. Portioli https://orcid.org/0000-0003-2711-3366
Michele Godio https://orcid.org/0000-0002-9586-8667
Chiara Calderini https://orcid.org/0000-0002-1525-5095
Paulo B. Lourenço https://orcid.org/0000-0001-8459-0199

REFERENCES
1. Lagomarsino S. Seismic assessment of rocking masonry structures. *Bull Earthq Eng*. 2015;13:97–128. https://doi.org/10.1007/s10518-014-9609-x
2. Sorrentino L, D'Ayala D, de Felice G, Griffith MC, Lagomarsino S, Magenes G. Review of out-of-plane seismic assessment techniques applied to existing masonry buildings. *Int J Archit Herit*. 2017;11:1-20. https://doi.org/10.1080/15583058.2016.1237586
3. CNTC. CIRCOLARE 21 gennaio 2019, n. 7 C.S.LL.PP. Istruzioni per l'applicazione dell'Aggiornamento delle "Norme tecniche per le costruzioni" di cui al decreto ministeriale 17 gennaio 2018. 2019.
4. NTC. Decreto Ministeriale 17/1/2018: Aggiornamento delle Norme tecniche per le costruzioni. Ministry of Infrastructures and Transportations; 2018.
5. Funari MF, Mehrotra A, Lourenço PB. A tool for the rapid seismic assessment of historic masonry structures based on limit analysis optimisation and rocking dynamics. *Appl Res*. 2021;11:1–22. https://doi.org/10.3390/app11030942
6. Reggiani Manzo N, Vassiliou MF. Displacement-based analysis and design of rocking structures. *Earthq Eng Struct Dyn*. 2019;48:1613–1629. https://doi.org/10.1002/eqe.3217
7. NTC. Decreto Ministeriale 14/1/2008: Norme tecniche per le costruzioni. Ministry of Infrastructures and Transportations; 2008.
8. Godio M, Beyer K. Evaluation of force-based and displacement-based out-of-plane seismic assessment methods for unreinforced masonry walls through refined model simulations. *Earthq Eng Struct Dyn*. 2019;48:454–475. https://doi.org/10.1002/eqe.3144
9. Doherty K, Griffith MC, Lam NTK, Wilson J. Displacement-based seismic analysis for out-of-plane bending of unreinforced masonry walls. *Earthq Eng Struct Dyn*. 2002;31:833–850. https://doi.org/10.1002/eqe.126
10. Griffith MC, Magenes G, Melis G, Picchi L. Evaluation of out-of-plane stability of unreinforced masonry walls subjected to seismic excitation. *J Earthq Eng*. 2003;7:141–169. https://doi.org/10.1080/13632460309350476
11. Calderini C, Lagomarsino S, Rossi M, De Canio G, Mongelli ML, Roselli I. Shaking table tests of an arch-pillars system and design of strengthening by the use of tie-rods. *Bull Earthq Eng*. 2015;13:279–297. https://doi.org/10.1007/s10518-014-9678-x
12. Griffith MC, Lam NTK, Wilson JL, Doherty K. Experimental investigation of unreinforced brick masonry walls in flexure. *J Struct Eng*. 2004;130:423-432. https://doi.org/10.1061/(ASCE)0733-9445(2004)130:3(423)
13. Shawa OA, de Felice G, Mauro A, Sorrentino L. Out-of-plane seismic behaviour of rocking masonry walls. *Earthq Eng Struct Dyn*. 2012;41:949–968. https://doi.org/10.1002/eqe.1168
14. Casapulla C, Giresini L, Lourenço PB. Rocking and kinematic approaches for rigid block analysis of masonry walls: state of the art and recent developments. *Buildings* 69, 2017;7. https://doi.org/10.3390/buildings7030069
15. Casapulla C, Argiento LU. The comparative role of friction in local out-of-plane mechanisms of masonry buildings. Pushover analysis and experimental investigation. *Eng Struct*. 2016;126:158–173. https://doi.org/10.1016/j.engstruct.2016.07.036
16. Giresini L, Fragiacomo M, Lourenço PB. Comparison between rocking analysis and kinematic analysis for the dynamic out-of-plane behavior of masonry walls. *Earthq Eng Struct Dyn*. 2015;44:2359–2376. https://doi.org/10.1002/eqe.2592
17. Godio M, Beyer K. Analytical model for the out-of-plane response of vertically spanning unreinforced masonry walls. *Earthq Eng Struct Dyn*. 2017;46:2757–2776. https://doi.org/10.1002/eqe.2929
18. D'Altri AM, Sarhosis V, Milani G, et al. Modeling strategies for the computational analysis of unreinforced masonry structures: review and classification. *Arch Comput Methods Eng*. 2020;27:1153–1185. https://doi.org/10.1007/s11831-019-09351-x
19. D'Altri AM, de Miranda S, Castellazzi G, Sarhosis V. A 3D detailed micro-model for the in-plane and out-of-plane numerical analysis of masonry panels. *Comput Struct*. 2018;206:18–30. https://doi.org/10.1016/j.compstruc.2018.06.007
20. de Felice G, Malena M. Failure pattern prediction in masonry. *J Mech Mater Struct*. 2019;14:663–682. https://doi.org/10.2140/jomms.2019.14.663

21. Milani G, Pizzolato M, Tralli A. Simple numerical model with second order effects for out-of-plane loaded masonry walls. *Eng Struct*. 2013;48:98–120. https://doi.org/10.1016/j.engstruct.2012.08.029

22. Chácara C, Cannizzaro F, Pantò B, Caliò I, Lourenço PB. Seismic vulnerability of URM structures based on a discrete macro-element modeling (DMEM) approach. *Eng Struct*. 2019;201:109715. https://doi.org/10.1016/j.engstruct.2019.109715

23. Pantò B, Cannizzaro F, Caddemi S, Caliò I. 3D macro-element modelling approach for seismic assessment of historical masonry churches. *Adv Eng Softw*. 2016;97:40–59. https://doi.org/10.1016/j.advengsoft.2016.02.009

24. Vanin F, Penna A, Beyer K. A three-dimensional macroelement for modelling the in-plane and out-of-plane response of masonry walls. *Earthq Eng Struct Dyn*. 2020;49:1365–1387. https://doi.org/10.1002/eqe.3277

25. Bui T-T, Limam A, Sarhosis V. Failure analysis of masonry wall panels subjected to in-plane and out-of-plane loading using the discrete element method. *Eur J Environ Civ Eng*. 2021;25:876–892. https://doi.org/10.1080/19648189.2018.1552897

26. de Felice G. Out-of-plane seismic capacity of masonry depending on wall section morphology. *Int J Archit Herit*. 2011;5:466–482. https://doi.org/10.1080/15583058.2010.530339

27. Ferrante A, Loverdos D, Clementi F, et al. Discontinuous approaches for nonlinear dynamic analyses of an ancient masonry tower. *Eng Struct*. 2021;230:111626. https://doi.org/10.1016/j.engstruct.2020.111626

28. Godio M, Beyer K. Quantifying the out-of-plane response of unreinforced masonry walls subjected to relative support motion. *Frat ed Integrità Strutt*. 2019;13:194–208. https://doi.org/10.3221/IGF-ESIS.50.17

29. Lemos JV. Discrete element modeling of masonry structures. *Int J Archit Herit*. 2007;1:190–213. https://doi.org/10.1080/15583050601176868

30. Malomo D, Pinho R, Penna A. Applied element modelling of the dynamic response of a full-scale clay brick masonry building specimen with flexible diaphragms. *Int J Archit Herit*. 2020;14:1484–1501. https://doi.org/10.1080/15583058.2019.1616004

31. Malomo D, Pinho R, Penna A. Numerical modelling of the out-of-plane response of full-scale brick masonry prototypes subjected to incremental dynamic shake-table tests. *Eng Struct*. 2020;209. https://doi.org/10.1016/j.engstruct.2020.110298

32. Sarhosis V, Baraldi D, Lemos JV, Milani G. Dynamic behaviour of ancient freestanding multi-drum and monolithic columns subjected to horizontal and vertical excitations. *Soil Dyn Earthq Eng*. 2019;120:39–57. https://doi.org/10.1016/j.soildyn.2019.01.024

33. Sarhosis V, Bagi K, Lemos JV, Milani G. *Computational modeling of masonry structures using the discrete element method*. IGI Global; 2016. https://doi.org/10.4018/978-1-5225-0231-9

34. D'Altri AM, Lo Presti N, Grillanda N, Castellazzi G, de Miranda S, Milani G. A two-step automated procedure based on adaptive limit and pushover analyses for the seismic assessment of masonry structures. *Comput Struct*. 2021;252:106561 https://doi.org/10.1016/j.compstruc.2021.106561

35. Portioli FPA. Rigid block modelling of historic masonry structures using mathematical programming: a unified formulation for non-linear time history, static pushover and limit equilibrium analysis. *Bull Earthq Eng*. 2020;18:211–239. https://doi.org/10.1007/s10518-019-00722-0

36. Angelillo M, Fortunato A, Gesualdo A, Iannuzzo A, Zuccaro G. Rigid block models for masonry structures. *Int J Mason Res Innov*. 2018;3:349–368. https://doi.org/10.1504/IJMRI.2018.095701

37. Baggio C, Trovalusci P. Collapse behaviour of three-dimensional brick-block systems using non-linear programming. *Struct Eng Mech*. 2000;10:181–195. https://doi.org/10.12989/sem.2000.10.2.181

38. Ferris MC, Tin-Loi F. Limit analysis of frictional block assemblies as a mathematical program with complementarity constraints. *Int J Mech Sci*. 2001;43:209–224. https://doi.org/10.1016/S0020-7403(99)00111-3

39. Gilbert M, Casapulla C, Ahmed HM. Limit analysis of masonry block structures with non-associative frictional joints using linear programming. *Comput Struct*. 2006;84:873–887. https://doi.org/10.1016/j.compstruc.2006.02.005

40. Nodargi NA, Intrigila C, Bisegna P. A variational-based fixed-point algorithm for the limit analysis of dry-masonry block structures with non-associative Coulomb friction. *Int J Mech Sci*. 2019;161-162. https://doi.org/10.1016/j.ijmecsci.2019.105078

41. Nodargi NA, Bisegna P. A unifying computational approach for the lower-bound limit analysis of systems of masonry arches and buttresses. *Eng Struct*. 2020;221. https://doi.org/10.1016/j.engstruct.2020.110999

42. Orduña A, Lourenço PB. Three-dimensional limit analysis of rigid blocks assemblages. Part I: Torsion failure on frictional interfaces and limit analysis formulation. *Int J Solids Struct*. 2005;42:5140–5160. https://doi.org/10.1016/j.ijsolstr.2005.02.010

43. Pepe M, Sangirardi M, Reccia E, Pingaro M, Trovalusci P, de Felice G. Discrete and continuous approaches for the failure analysis of masonry structures subjected to settlements. *Front Built Environ*. 2020;6. https://doi.org/10.3389/fbuil.2020.00043

44. Iannuzzo A, Dell'Endice A, Van Mele T, Block P. Numerical limit analysis-based modelling of masonry structures subjected to large displacements. *Comput Struct*. 2021;242. https://doi.org/10.1016/j.compstruc.2020.106372

45. Portioli F, Cascini L. Large displacement analysis of dry-jointed masonry structures subjected to settlements using rigid block modelling. *Eng Struct*. 2017;148:485–496. https://doi.org/10.1016/j.engstruct.2017.06.073

46. Tralli A, Chiozzi A, Grillanda N, Milani G. Masonry structures in the presence of foundation settlements and unilateral contact problems. *Int J Solids Struct*. 2020;191-192:187–201. https://doi.org/10.1016/j.ijsolstr.2019.12.005

47. Sarhosis V, Garrity SW, Sheng Y. Influence of brick–mortar interface on the mechanical behaviour of low bond strength masonry brickwork lintels. *Eng Struct*. 2015;88:1–11. https://doi.org/10.1016/j.engstruct.2014.12.014

48. Lu M, Schultz AE, Stolarski HK. Analysis of the influence of tensile strength on the stability of eccentrically compressed slender unreinforced masonry walls under lateral loads. *J Struct Eng*. 2004;130:921–933. https://doi.org/10.1061/(ASCE)0733-9445(2004)130:6(921)

49. Ferrero C, Calderini C, Portioli F, Roca P. Large displacement analysis of dry-joint masonry arches subject to inclined support movements. *Eng Struct*. 2021;238:112244. https://doi.org/10.1016/j.engstruct.2021.112244

50. Gagliardo R, Portioli FPA, Cascini L, Landolfo R, Lourenço PB. A rigid block model with no-tension elastic contacts for displacement-based assessment of historic masonry structures subjected to settlements. *Eng Struct*. 2021;229. https://doi.org/10.1016/j.engstruct.2020.111609

51. Itasca Consulting Group. UDEC 6.0. 2014.

52. Calderini C, Lagomarsino S. Seismic response of masonry arches reinforced by tie-rods: static tests on a scale model. *J Struct Eng*. 2015;141. https://doi.org/10.1061/(ASCE)ST.1943-541X.0001079

53. Lourenço PB, Oliveira DV, Roca P, Orduña A. Dry joint stone masonry walls subjected to in-plane combined loading. *J Struct Eng*. 2005;131:1665–1673. https://doi.org/10.1061/(ASCE)0733-9445(2005)131:11(1665)

54. Mehrotra A, DeJong MJ. The influence of interface geometry, stiffness, and crushing on the dynamic response of masonry collapse mechanisms. *Earthq Eng Struct Dyn*. 2018;47:2661–2681. https://doi.org/10.1002/eqe.3103

55. Livesley RK. A computational model for the limit analysis of three-dimensional masonry structures. *Meccanica*. 1992;27:161–172. https://doi.org/10.1007/BF00430042

56. Derakhshan H, Griffith MC, Ingham JM. Out-of-plane seismic response of vertically spanning URM walls connected to flexible diaphragms. *Earthq Eng Struct Dyn*. 2016;45:563–580. https://doi.org/10.1002/eqe.2671

57. Godio M, Beyer K. Trilinear model for the out-of-plane seismic assessment of vertically spanning unreinforced masonry walls. *J Struct Eng*. 2019;145. https://doi.org/10.1061/(ASCE)ST.1943-541X.0002443

58. Giouvanidis AI, Dimitrakopoulos EG. Nonsmooth dynamic analysis of sticking impacts in rocking structures. *Bull Earthq Eng*. 2017;15:2273–2304. https://doi.org/10.1007/s10518-016-0068-4

59. Krabbenhoft K, Lyamin AV, Huang J, Vicente da Silva M. Granular contact dynamics using mathematical programming methods. *Comput Geotech*. 2012;43:165–176. https://doi.org/10.1016/j.compgeo.2012.02.006

60. Krabbenhoft K, Huang J, Da Silva MV, Lyamin AV. Granular contact dynamics with particle elasticity. *Granul Matter*. 2012;14:607–619. https://doi.org/10.1007/s10035-012-0360-1

61. Lloyd Smith D. *Mathematical Programming Methods in Structural Plasticity*. Vienna: Springer; 1990.

62. Meng J, Huang J, Sheng D, Sloan SW. Granular contact dynamics with elastic bond model. *Acta Geotech*. 2017;12:479–493. https://doi.org/10.1007/s11440-016-0481-5

63. Cottle RW, Pang JS, Stone RE. *The linear complementarity problem*. SIAM; 2009.

64. Portioli F, Casapulla C, Cascini L. An efficient solution procedure for crushing failure in 3D limit analysis of masonry block structures with non-associative frictional joints. *Int J Solids Struct*. 2015;69-70:252–266. https://doi.org/10.1016/j.ijsolstr.2015.05.025

65. Portioli F, Cascini L, Casapulla C, D'Aniello M. Limit analysis of masonry walls by rigid block modelling with cracking units and cohesive joints using linear programming. *Eng Struct*. 2013;57:232–247. https://doi.org/10.1016/j.engstruct.2013.09.029

66. Bleyer J, de Buhan P. A computational homogenization approach for the yield design of periodic thin plates. Part I: Construction of the macroscopic strength criterion. *Int J Solids Struct*. 2014;51:2448–2459. https://doi.org/10.1016/j.ijsolstr.2014.03.018

67. El Boustani C, Bleyer J, Arquier M, Ferradi MK, Sab K. Dual finite-element analysis using second-order cone programming for structures including contact. *Eng Struct*. 2020;208:109892. https://doi.org/10.1016/j.engstruct.2019.109892

68. Maier G, Nappi A. A theory of no-tension discretized structural systems. *Eng Struct*. 1990;12:227–234. https://doi.org/10.1016/0141-0296(90)90021-J

69. Baggio C, Trovalusci P. Limit analysis for no-tension and frictional three-dimensional discrete systems*. *Mech Struct Mach*. 1998;26:287–304. https://doi.org/10.1080/08905459708945496

70. Azevedo J, Sincraian G, Lemos JV. Seismic behavior of blocky masonry structures. *Earthq Spectra*. 2000;16:337–365. https://doi.org/10.1193/1.1586116

71. Orduña A, Lourenço PB. Cap model for limit analysis and strengthening of masonry structures. *J Struct Eng*. 2003;129:1367–1375. https://doi.org/10.1061/(ASCE)0733-9445(2003)129:10(1367)

72. Portioli F, Casapulla C, Cascini L, D'Aniello M, Landolfo R. Limit analysis by linear programming of 3D masonry structures with associative friction laws and torsion interaction effects. *Arch Appl Mech*. 2013;83:1415–1438. https://doi.org/10.1007/s00419-013-0755-4

73. D'Altri AM, de Miranda S, Milani G, Castellazzi G. A numerical procedure for the force-displacement description of out-of-plane collapse mechanisms in masonry structures. *Comput Struct*. 2020;233:106234. https://doi.org/10.1016/j.compstruc.2020.106234